Atmos. Chem. Phys. Discuss., 13, 12725–12742, 2013
www.atmos-chem-phys-discuss.net/13/12725/2013/
doi:10.5194/acpd-13-12725-2013

Atmospheric Chemistry and Physics Discussions
Open Access

The impact of horizontal heterogeneities, cloud fraction, and cloud dynamics on warm cloud effective radii and liquid water path from CERES-like Aqua MODIS retrievals

D. Painemal[1], P. Minnis[1], and S. Sun-Mack[2]

[1]NASA Langley Research Center, Hampton, Virginia, USA
[2]Science System and Applications Inc., Hampton, Virginia, USA

Received: 25 April 2013 – Accepted: 1 May 2013 – Published: 14 May 2013

Correspondence to: D. Painemal (david.painemal@nasa.gov)

Published by Copernicus Publications on behalf of the European Geosciences Union.

Abstract

The impact of horizontal heterogeneities, liquid water path (LWP from AMSR-E), and cloud fraction (CF) on MODIS cloud effective radius (r_e), retrieved from the 2.1 µm ($r_{e2.1}$) and 3.8 µm ($r_{e3.8}$) channels, is investigated for warm clouds over the southeast Pacific. Values of r_e retrieved using the CERES Edition 4 algorithms are averaged at the CERES footprint resolution (~20 km), while heterogeneities (H_σ) are calculated as the ratio between the standard deviation and mean 0.64 µm reflectance. The value of $r_{e2.1}$ strongly depends on CF, with magnitudes up to 5 µm larger than those for overcast scenes, whereas $r_{e3.8}$ remains insensitive to CF. For cloudy scenes, both $r_{e2.1}$ and $r_{e3.8}$ increase with H_σ for any given AMSR-E LWP, but $r_{e2.1}$ changes more than for $r_{e3.8}$. Additionally, $r_{e3.8} - r_{e2.1}$ differences are positive (< 1 µm) for homogeneous scenes ($H_\sigma < 0.2$) and LWP > 50 g m^{-2}, and negative (up to −4 µm) for larger H_σ. Thus, $r_{e3.8} - r_{e2.1}$ differences are more likely to reflect biases associated with cloud heterogeneities rather than information about the cloud vertical structure. The consequences for MODIS LWP are also discussed.

1 Introduction

Cloud optical thickness (τ) and effective radius (r_e) derived from visible and near-infrared satellite instruments have become the standard observational dataset in cloud-atmospheric research. The availability of these parameters at high temporal and spatial resolution over the globe over long time periods makes them particularly suitable for climate studies (e.g., Stubenrauch et al., 2013). Among several practical simplifications that make the inverse problem of determining r_e and τ tractable, is the assumption that clouds are horizontally homogeneous (plane-parallel) objects. Nevertheless, the effect of neglecting the cloud 3-D structure and the associated radiative fields can be a significant source of retrievals error (Marshak et al., 2006). Given this uncertainty, there is an increasing interest in understanding how the 3-D radiative effects can obscure the physical insight gained from satellite observations.

Multi-spectral instruments such as the MODerate resolution Imaging Spectroradiometer (MODIS) offer practical ways to explore 3-D related artifacts in the retrievals. Since 3-D radiative effects are wavelength dependent, the use of three MODIS r_e retrievals from the 1.6, 2.1, and 3.8 µm channels, provides a simple framework to explore biases in the observations (e.g., Zhang and Platnick, 2011). Although in principle r_e retrieved at 3.8 µm is less sensitive to plane-parallel biases and 3-D radiative effects, determining the effects of cloud heterogeneities with the use of multispectral r_e retrievals is difficult as the different photon penetration of the three MODIS channels in theory should also capture physical information of the cloud vertical structure (Platnick, 2000). This implies that the 3.8 µm-based r_e is more influenced by properties closer to the cloud top than the 2.1 and 1.6 µm counterparts.

In this contribution, we explore the ways that cloud properties retrieved from Aqua MODIS radiances vary for different cloud dynamical configurations and spatial heterogeneities at spatial resolutions typical of synoptic/climate studies. The goal here is to determine the bias magnitude in r_e due to heterogeneities as well as understanding the physical information that can be obtained from r_e differences calculated at two wavelengths (3.8 and 2.1 µm).

2 Dataset

Here we use values of τ and r_e retrieved from Aqua MODIS data using algorithms that will be used generate the Clouds and Earth's Radiant Energy System (CERES) Edition-4 products and averaged in the same manner as the CERES Single Scanner Footprint (SSF) product (CERES, 2012) to create a pseudo-SSF, hereafter, PSSF. The Edition-4 algorithm changes relative to the CERES Edition-2 techniques (Minnis et al., 2011a) are mostly summarized by Minnis et al. (2010). The cloud parameters are derived from 1 km MODIS radiances sampled every other scan line and fourth

ACPD
13, 12725–12742, 2013

element, and convolved with the CERES instrument point spread function to produce averages and standard deviations that match the CERES instrument footprint (∼ 20 km at nadir). The PSSF used here includes several hundred parameters including averages and standard deviations of the MODIS radiances, τ retrieved at 0.64 µm, and three r_e values retrieved from the 1.2, 2.1, and 3.8 µm MODIS channels. The multispectral retrievals for r_e use the same method as that described by Minnis et al. (2011) to obtain r_e at 3.8 µm, $r_{e3.8}$, except that the 1.2 and 2.1 µm reflectances substitute for the 3.8 µm brightness temperatures in the iterative solution to yield $r_{e1.2}$ and $r_{e2.1}$, respectively. In this investigation we only use the 3.8 and 2.1 µm-based r_e, because they have proven to yield contrasting sensitivities to both the cloud vertical and horizontal structure (Platnick, 2000; Zhang and Platnick, 2011). The 1.2 µm-based r_e retrieval is still experimental and will require further evaluation before being used for scientific analyses. Cloud fraction (CF) is also convolved from the clear and cloudy MODIS pixels within each CERES footprint. Although the CERES cloud algorithm differs from that of the MODIS Atmospheres team (Platnick et al., 2005), both results agree well for $r_{e3.8}$, with some small differences mainly explained by the tendency of the MODIS team Collection 5 retrievals to discard pixels with very thin clouds or near the cloud edges in broken scenes (Minnis et al., 2011b). Figure 1a shows the mean CERES $r_{e3.8}$ (colors) and $\Delta r_e = r_{e3.8} - r_{e2.1}$ (contours) during the period of study. The $r_{e3.8}$ values agree with MODIS team counterpart in Zhang and Platnick (2011) and Nakajima et al. (2010), in terms of magnitude and westward gradient. Moreover, as in the MODIS team retrievals, $r_{e2.1}$ is generally larger than $r_{e3.8}$, with a westward increase of $|\Delta r_e|$ (Fig. 1a, contours), consistent with larger liquid water paths as well (O'Dell et al., 2008). These features are also common to other marine stratocumulus regimes (Zhang and Platnick, 2010).

We computed a heterogeneity index H_σ, defined as the ratio of the standard deviation to the mean MODIS 0.64 µm reflectance at the PSSF resolution (∼ 20 km at nadir). We note that H_σ defined here differs from that in Zhang and Platnick (2011), which is calculated at a 1 km resolution from the 0.86 µm MODIS reflectances. While 1 km H_σ is more adequate for studying 3-D radiative effects, the use of a coarser H_σ is relevant for

ACPD
13, 12725–12742, 2013

determining how spatial heterogeneities might bias the retrievals at typical resolutions used in regional/climate studies.

Finally, as explained in Painemal et al. (2012), in order to create regular-grid maps, we spatially average the PSSF variables to a resolution of 0.5 (each new grid contains at least one PSSF near the scan edge).

Independent liquid water path LWP retrievals are from the Advanced Microwave Scanning Radiometer-EOS, AMSR-E (Wentz and Meissner, 2000), and spatially averaged to a 0.5° spatial resolution from the 0.25° native resolution. In order to minimize precipitation biases in AMSR-E LWP, we limited our analysis to clouds with LWP $< 150\,\mathrm{g\,m^{-2}}$. While this threshold screens cases with moderate and heavy precipitation, it still allows cloud sampling with light precipitation (e.g., Leon et al., 2009).

As in Zhang and Platnick (2011), our focus is on the marine stratocumulus regime of the Southeast Pacific, defined here as encompassing the oceanic area within the bounds, 100–70° W, 33–5° S. We analyze 15 months of daily satellite passes during the August–December period, when the cloud deck is at its maximum spatial development, from 2002 to 2004. The solar zenith angles between 20° and 35° allow us to isolate the effect of cloud heterogeneities from the solar zenith angle influence in the retrievals, especially for very oblique angles (Kato and Marshak, 2009).

3 Cloud fraction and heterogeneity

Mean H_σ shows typical values between 0.1 and 0.4, with increasing heterogeneities westward (Fig. 1b). As expected, H_σ and CF spatially co-vary, with a decrease in cloud fraction generally concomitant with larger H_σ. The spatial similarities between r_e, Δr_e, H_σ, and CF motivate a more detailed inspection of the factors that control Δr_e.

The histogram in Fig. 2a shows that the scene heterogeneity tends to increase with CF until CF reaches 60 %. For higher CFs, H_σ is anti-correlated with CF, whereas for nearly overcast scenes, the liquid water path modulates H_σ, as shown in the following sections. Figure 2b and c depicts the binned values of $r_{e3.8}$ and $r_{e2.1}$ as functions of

Discussion Paper | Discussion Paper | Discussion Paper | Discussion Paper |

ACPD
13, 12725–12742, 2013

The impact of cloud heterogeneities in MODIS retrievals

D. Painemal et al.

CF and H_σ. As expected, the general trend is that both $r_{e3.8}$ and $r_{e2.1}$ increase with H_σ, reaching their largest magnitude for $H_\sigma = 0.4$. Nevertheless, both retrievals show dissimilar sensitivities to changes in CF. While $r_{e3.8}$ is insensitive to CF variations, $r_{e2.1}$ decreases with CF, with radii between 12–17 µm for a fixed $H_\sigma = 0.2$. It can also be seen that the $r_{e3.8} - r_{e2.1}$ difference (Δr_e) is near –6 µm for $H_\sigma < 0.15$ and CF = 40 %, whereas this is reduced to around −1 to −2 µm for overcast scenes only. These results strongly support the observations made by Zhang and Platnick (2011) for a limited number of overcast and broken MODIS granules. The values of Δr_e, as a function of CF and H_σ, are in agreement with the smaller impact of 3-D radiative transfer and sub-pixel variability on $r_{e3.8}$ than on $r_{e2.1}$, although the negligible impact of CF on $r_{e3.8}$ is surprising.

4 Heterogeneity and AMSR-E liquid water path in cloudy scenes

For cloudy scenes, when CF > 98 %, an LWP-dependent analysis is essential because one should expect a relationship between LWP, H_σ, and the cloud vertical structure. The latter is associated with the fact that a greater LWP yields more vigorous up and down drafts, active collision-coalescence, and, therefore, a larger r_e and potential drizzle (e.g., Leon et al., 2008). To tackle the problem of untangling the heterogeneity bias from the physical information, we use AMSR-E LWP, a retrieval that is insensitive to 3-D radiative transfer effects. Similar to the approach in Sect. 3, we binned the MODIS retrievals as functions of both H_σ and AMSR-E LWP. Figure 3a shows the dual dependence of $r_{e3.8}$ on H_σ and LWP. Irrespective of H_σ, $r_{e3.8}$ increases with LWP, which is consistent with more active collision and coalescence when water content increases. In addition, $r_{e3.8}$ increases with H_σ are also apparent, in agreement with other studies (Zhang and Platnick, 2011; Zhang et al., 2012). The magnitude of the change in $r_{e3.8}$ with H_σ is confined to 3–4 µm for any given LWP bin.

Differences between $r_{e3.8}$ and $r_{e2.1}$ are depicted in Fig. 3b. The largest differences, near 4 µm, are observed for the most heterogeneous cases, irrespective of

LWP. For $H_\sigma = 0.1$, Δr_e is small, with positive values for LWP > 50 g m^{-2} (~0.8 µm for LWP = 125 g m^{-2}). Larger values of $r_{e3.8}$ relative to those for $r_{e2.1}$ are consistent with aircraft observations over this region, which show that r_e monotonically increases with height until reaching its maximum at the cloud top (Painemal and Zuidema, 2011). Finally, Fig. 3c shows the expected decrease of τ with increasing H_σ, as well as the optical thickening with increasing LWP.

5 Revisiting the impact of H_σ on MODIS liquid water path

Because the product of r_e and τ can be used to estimate LWP, we center our focus on LWP. Here, we express the MODIS LWP by assuming a cloud having a vertical increase of water content and r_e with height:

$$\text{MODIS LWP} = \frac{5}{9}\rho_w \cdot r_e \cdot \tau, \tag{1}$$

where ρ_w denotes the density of the liquid water. LWP in Eq. (1) is 5/6 the magnitude of that calculated for a vertically homogeneous cloud and it is adopted here because it yields better agreement with microwave estimates (Seethala and Horvath, 2010).

Figure 4 shows the binned MODIS LWP, $LWP_{3.8}$, and $LWP_{2.1}$, using $r_{e3.8}$ and $r_{e2.1}$, respectively, as a function of AMSR-E LWP only. In addition, the binned H_σ is also reported (blue line, and right axis). The MODIS-AMSR-E mean bias and root mean square pairs are, respectively, 4.8 and 18.3 g m^{-2} for $LWP_{3.8}$, and 7.3 and 17.6 g m^{-2} for $LWP_{2.1}$. Because $r_{e3.8}$ is, on average, smaller than $r_{e2.1}$, $LWP_{3.8}$ yields a slightly smaller mean bias, particularly for LWP < 110 g m^{-2}. In contrast, MODIS biases become negative for AMSR-E LWP > 110 gm^2. A similar finding was observed by Painemal et al. (2012) between the Tenth Geostationary Operational Environmental Satellite (GOES-10) and the TRMM Microwave Imager (TMI) LWP values. The bias sign shift is also in qualitative agreement with the annual maps of Seethala and Horvath (2010) over maritime stratocumulus regimes. They found that the MODIS LWP exceeded its AMSR-E counterpart near the coast, whereas the opposite was observed 15° offshore. This westward change also co-occurs with a westward increase of the mean LWP. The causes of a LWP dependence on MODIS-AMSR-E bias seems to be related to the increasing cloud heterogeneities with increasing LWP, as depicted in Fig. 4 (blue line). Smaller values of MODIS LWP compared to their AMSR-E counterparts for high H_σ implies that increases in r_e cannot completely offset the decrease in τ for heterogeneous clouds. We explore this idea in more detail by taking averages of all LWP bins as a function of H_σ bins. The results in Fig. 5a reveal the close match between $r_{e2.1}$ and $r_{e3.8}$ for homogeneous cases and the greater increase of $r_{e2.1}$ with H_σ (black and red lines). In terms of LWP (Fig. 5b), decreases in MODIS LWP with H_σ are more dramatic for $\mathrm{LWP}_{3.8}$. Here, the AMSR-E LWP is constant at $80\,\mathrm{g\,m^{-2}}$ by design.

We quantify the influence of H_σ by analyzing fractional changes of MODIS LWP relative to fractional changes in H_σ, $\frac{\partial \ln(\mathrm{LWP}_\kappa)}{\partial \ln(H_\sigma)}$, with $\kappa = 3.8, 2.1$. It follows from Eq. (1) that:

$$\underbrace{\frac{\partial \ln(\mathrm{LWP}_\kappa)}{\partial \ln(H_\sigma)}}_{m_{\mathrm{LWP}_\kappa}} = \underbrace{\frac{\partial \ln(r_{e\kappa})}{\partial \ln(H_\sigma)}}_{m_{r\kappa}} + \underbrace{\frac{\partial \ln(\tau)}{\partial \ln(H_\sigma)}}_{m_\tau} \tag{2}$$

where m_{LWP_κ}, $m_{r\kappa}$, and m_τ in Eq. (2), are calculated as the slopes of the natural logarithm of the curves in Fig. 5a and b (Table 1). As a consistency check, we compared the calculated left and right hand sides in Eq. (2) and found that the combined r_e and τ slopes depart by less than 24 % from those for LWP. In terms of the r_e slopes, $m_{r3.8}$ is smaller than $m_{r2.1}$ (0.34) by 50 %. The dominant dependence of LWP on τ and the negative sign of the $\ln(\tau) - \ln(H_\sigma)$ slope ($m_\tau = -0.44$) explains why the MODIS LWP decreases with H_σ, and the LWP bias decreases and changes sign with AMSR-E LWP (Figs. 5b and 4, respectively). The values in Table 1 also help explain why changes in $\mathrm{LWP}_{2.1}$ with H_σ are smaller than those for $\mathrm{LWP}_{3.8}$.

ACPD
13, 12725–12742, 2013

6 Conclusions

Motivated by studies that support both the physical and the 3-D-radiative interpretation of the r_e differences at the 3.8 and 2.1 µm MODIS channels, we endeavored to understand the contribution of LWP and H_σ to the Δr_e variability. Homogeneous clouds have larger values of $r_{e3.8}$ relative to $r_{e2.1}$, indicating a physical increase of r_e toward the cloud top and a negligible effect of precipitation in the retrievals, contrary to the findings in Nakajima et al. (2010). Our results are consistent with aircraft observations of cloud microphysics over the region of study, which show an adiabatic-like cloud behavior (Painemal and Zuidema, 2011). The current study also shows that the use of Δr_e for microphysical studies without knowledge of H_σ will lead to spurious results. Because H_σ typically increases with LWP, cumulus-like clouds will continue to pose a formidable challenge for passive remote sensing. Overall, we conclude that Δr_e is more suitable as a metric to investigate cloud heterogeneities rather than the cloud physical structure in marine stratocumulus clouds.

A result of interest for cloud-aerosol interaction studies is the lack of sensitivity of $r_{e3.8}$ to CF. Although a weaker dependence of $r_{e3.8}$ on CF is expected from the reduced photon vertical penetration at 3.8 µm and from the smaller sensitivity to sub-pixel variability (plane-parallel bias) than retrievals at 2.1 µm, the negligible dependence of $r_{e3.8}$ on CF is rather unexpected. We hypothesize that this is related to the fact that our observations are $0.5^\circ \times 0.5^\circ$ averages, which allow further error cancellation (e.g., Marshak et al., 2006). We recommend caution when using $r_{e2.1}$ combined with nearly collocated aerosol optical thickness, especially if broken clouds dominate the r_e retrieval scenes. A similar problem might arise if variability in $r_{e2.1}$ is analyzed as a function of meteorological factors, since they are likely to be correlated with cloud cover variability (e.g., Lebsock et al., 2008).

The problem of determining errors in MODIS-based LWP is difficult because of the dissimilar responses of r_e and τ to changes in cloud heterogeneities. Our results also provide interpretation of the AMSR-MODIS LWP bias correlation with Δr_e reported by

Discussion Paper | Discussion Paper | Discussion Paper | Discussion Paper |

ACPD

13, 12725–12742, 2013

The impact of cloud heterogeneities in MODIS retrievals

D. Painemal et al.

Seethala and Horvath (2010). The smaller values of MODIS LWP relative to the AMSR-E values, when $r_{e2.1}$ greatly exceeds $r_{e3.8}$, are associated with the rapid decrease of τ with H_σ as the AMSR-E LWP increases. It is still puzzling why the MODIS LWP is slightly larger than AMSR-E LWP for highly homogeneous cases. A plausible cause might be linked to the thermal emission underestimation within the AMSR-E LWP algorithm (Seethala and Horvath, 2010), although unexplained overestimates of MODIS r_e relative to in-situ observations (Painemal and Zuidema, 2011) might also contribute to overestimates of MODIS LWP relative to AMSR-E LWP.

Concerning plausible ways to ameliorate the MODIS bias, regressions between MODIS LWP and H_σ for different LWP bins might be used to remove the H_σ dependence in operational retrievals. Nevertheless, other considerations such as solar zenith angle dependence, cloud cover variability or potential biases in the microwave dataset have to be carefully considered before attempting a LWP correction for operational purposes.

Acknowledgements. D. Painemal was supported by the NASA Postdoctoral Program at the NASA Langley Research Center. P. Minnis and S. Sun-Mack were supported by the NASA Modeling, Analysis, and Prediction and CERES Programs. The CERES-like PSSF data were processed at the NASA Earth Observing System Data and Information System, Langley Research Center Atmospheric Sciences Data Center. AMSR-E data are produced by Remote Sensing Systems and sponsored by the NASA Earth Science MEaSUREs DISCOVER Project and the AMSR-E Science Team. Data are available at http://www.remss.com.

References

CERES: Single scanner footprint TOA/surface fluxes and clouds (SSF), CERES Data Products Catalog, DPC-SSF-Ed4 R5V, 16 pp., 2012.

Kato, S. and Marshak, A.: Solar zenith and viewing geometry-dependent errors in satellite retrieved cloud optical thickness: marine stratocumulus case, J. Geophys. Res., 114, D01202, doi:10.1029/2008JD010579, 2009.

Lebsock, M. D., Stephens, G. L., and Kummerow, C.: Multisensor satellite observations of aerosol effects on warm clouds, J. Geophys. Res., 113, D15205, doi:10.1029/2008JD009876, 2008.

Leon, D. C., Wang, Z., and Liu, D.: Climatology of drizzle in marine boundary layer clouds based on 1 year of data from CloudSat and Cloud-Aerosol Lidar and Infrared Pathfinder Satellite Observations (CALIPSO), J. Geophys. Res., 113, D00A14, doi:10.1029/2008JD009835, 2008.

Marshak, A., Platnick, S., Várnai, T., Wen, G., and Cahalan, R. F.: Impact of three-dimensional radiative effects on satellite retrievals of cloud droplet sizes, J. Geophys. Res., 111, D09207, doi:10.1029/2005JD006686, 2006.

Minnis, P., Sun-Mack, S., Trepte, Q. Z., Chang F.-L., Heck, P. W., Chen, Y., Yi, Y., Arduini, R. F., Ayers, K., Bedka, K., Bedka, S., Brown, R., Gibson, S., Heckert, E., Hong, G., Jin, Z., Palikonda, R., Smith, R., Smith, W., Spangenberg, D., Yang, P., and Yost, C. X. Y.: CERES Edition 3 cloud retrievals, in: Proc. AMS 13th Conf. Atmos. Rad., Portland, OR, 27 June–2 July, 5.4, 2010.

Minnis, P., Sun-Mack, S., Young, D. F., Heck, P. W., Garber, D. P., Chen, Y., Spangenberg, D. A., Arduini, R. F., Trepte, Q. Z., Smith Jr., W. L., Ayers, J. K., Gibson, S. C., Miller, W. F., Chakrapani, V., Takano, Y., Liou, K.-N., and Xie, Y.: CERES Edition-2 cloud property retrievals using TRMM VIRS and Terra and Aqua MODIS data – Part I: Algorithms, IEEE T. Geosci. Remote Se., 49, 4374–4400, doi:10.1109/TGRS.2011.2144601, 2011a.

Minnis, P., Sun-Mack, S., Chen, Y., Khaiyer, M. M., Yi, Y., Ayers, J. K., Brown, R. R., Dong, X., Gibson, S. C., Heck, P. W., Lin, B., Nordeen, M. L., Nguyen, L., Palikonda, R., Smith, W. L., Spangenberg, D. A., Trepte, Q. Z., and Xi, B.: CERES Edition-2 cloud property retrievals using TRMM VIRS and Terra and Aqua MODIS data – Part II: Examples of average results and comparisons with other data, IEEE T. Geosci. Remote Se., 49, 4401–4430, doi:10.1109/TGRS.2011.2144602, 2011b.

Nakajima, T. Y., Suzuki, K., and Stephens, G. L.: Droplet growth in warm water clouds observed by the A-Train – Part II: A multisensor view, J. Atmos. Sci., 67, 1897–1907, doi:10.1175/2010JAS3276.1, 2010.

O'Dell, C. W., Wentz, F. J., and Bennartz, R.: Cloud liquid water path from satellite-based passive microwave observations: a new climatology over the global oceans, J. Climate, 21, 1721–1739, 2008.

ACPD
13, 12725–12742, 2013

Painemal, D. and Zuidema, P.: Assessment of MODIS cloud effective radius and optical thickness retrievals over the Southeast Pacific with VOCALS-Rex in-situ measurements, J. Geophys. Res., 116, D24206, doi:10.1029/2011JD016155, 2011.

Painemal, D., Minnis, P., Ayers, J. K., and O'Neill, L.: GOES-10 microphysical retrievals in marine warm clouds: multi-instrument validation and daytime cycle over the southeast Pacific, J. Geophys. Res., 117, D19212, doi:10.1029/2012JD017822, 2012.

Platnick, S.: Vertical photon transport in cloud remote sensing problems, J. Geophys. Res., 105, 22919–22935, doi:10.1029/2000JD900333, 2000.

Platnick, S., King, M., Ackerman, S., Menzel, W., Baum, B., Riedi, J., and Frey, R.: The MODIS cloud products: algorithms and examples from Terra, IEEE T. Geosci. Remote Se., 41, 459–473, doi:10.1109/TGRS.2002.808301, 2003.

Seethala, C. and Horváth, Á.: Global assessment of AMSR-E and MODIS cloud liquid water path retrievals in warm oceanic clouds, J. Geophys. Res., 115, D13202, doi:10.1029/2009JD012662, 2010.

Stubenrauch, C., Rossow, W. B., Kinne, S., Ackerman, S., Cesana, G., Chepfer, H., Di Girolamo, L., Getzewich, B., Guignard, A., Heidinger, A., Maddux, B. C., Menzel, W. P., Minnis, P., Pearl, C., Platnick, S., Poulsen, C., Riedi, J., Sun-Mack, S., Walther, A., Winker, D., Zeng, S., and Zhao, G.: Assessment of global cloud datasets from satellites: project and database initiated by the GEWEX Radiation Panel, B. Am. Meteorol. Soc., 94, in press, 2013.

Wentz, F. and Meissner, T.: AMSR Ocean Algorithm, Algorithm Theor. Basis Doc. 121599A-1, Remote Sens. Syst., Santa Rosa, CA, 2000.

Zhang, Z. and Platnick, S.: An assessment of differences between cloud effective particle radius retrievals for marine water clouds from three MODIS spectral bands, J. Geophys. Res., 116, D20215, doi:10.1029/2011JD016216, 2011.

Zhang, Z., Ackerman, A. S., Feingold, G., Platnick, S., Pincus, R., and Xue, H.: Effects of cloud horizontal inhomogeneity and drizzle on remote sensing of cloud droplet effective radius: case studies based on large-eddy simulations, J. Geophys. Res., 117, D19208, doi:10.1029/2012JD017655, 2012.

Table 1. MODIS fractional changes relative to fractional changes in H_σ, Eq. (2).

	$m_{\mathrm{LWP}\kappa}$	$m_{r\kappa} + m_\tau$	$m_{r\kappa}$	m_τ
$\kappa = 3.8$	−0.29	−0.27	0.17	-0.44
$\kappa = 2.1$	−0.13	−0.10	0.34	

ACPD
13, 12725–12742, 2013

The impact of cloud heterogeneities in MODIS retrievals

D. Painemal et al.

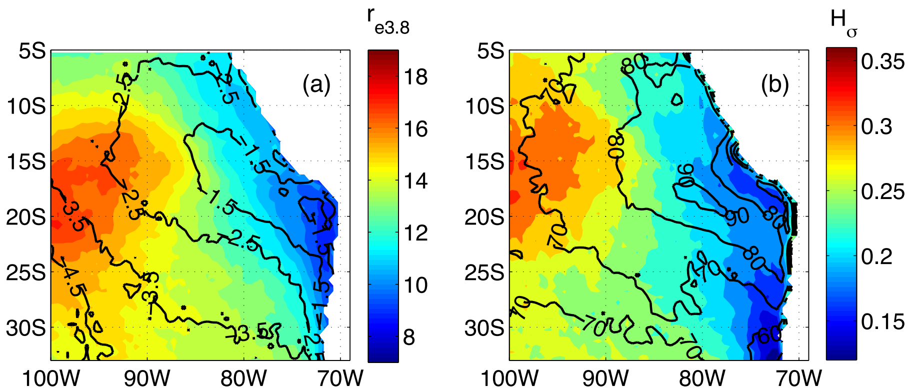

Fig. 1. Average fields during the period of study: **(a)** $r_{e3.8}$ (color) and $\Delta r_e = r_{e3.8} - r_{e2.1}$ (contours), **(b)** H_σ (colors) and cloud fractions (contours). The continent is represented by the white region.

ACPD
13, 12725–12742, 2013

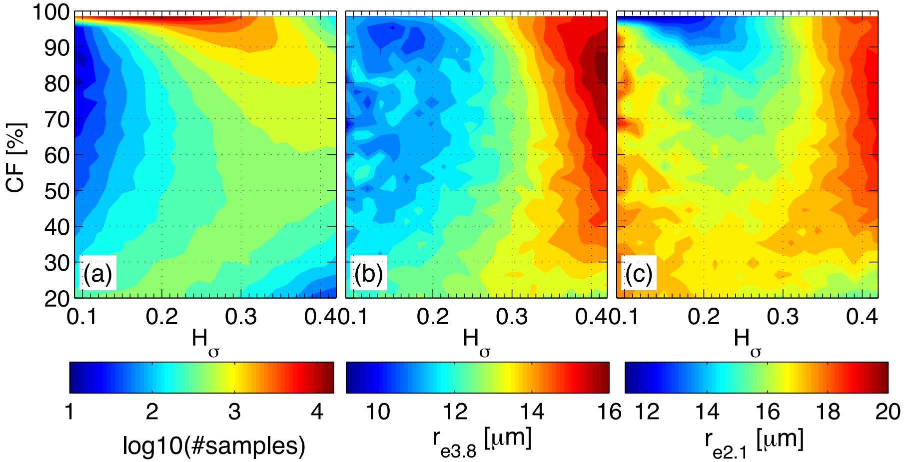

Fig. 2. (a) Number of samples contained in each H_σ-CF bin (logarithmic scale). **(b)** Mean $r_{e3.8}$ for each H_σ-CF bin, **(c)** same as Fig. 1b but for $r_{e2.1}$. The bin sizes are 3 % and 0.016 for CF and H_σ, respectively.

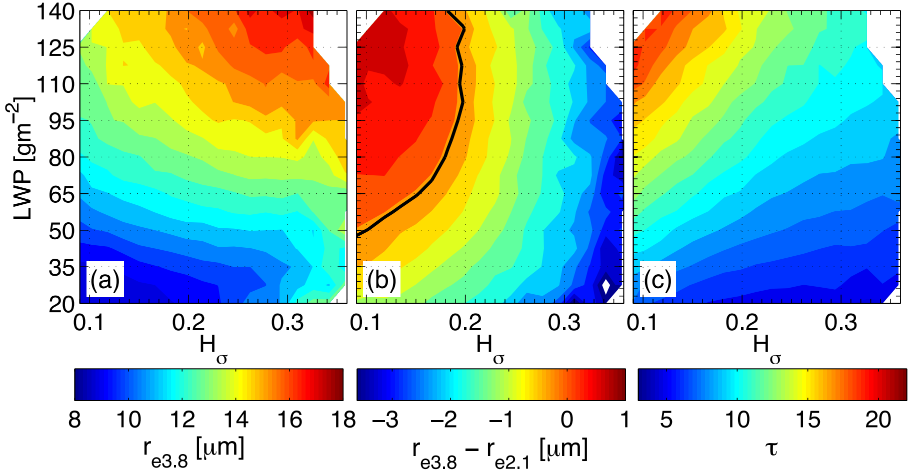

Fig. 3. Binned values for cloudy scenes (CF > 98 %) as a function of H_σ and AMSR-E LWP: **(a)** $r_{e3.8}$, **(b)** $\Delta r_e = r_{e3.8} - r_{e2.1}$, with zero values denoted by the black contour, and **(c)** τ. The bin sizes are 0.016 and 7.5 g m^{-2} for CF and H_σ, respectively. Bins constructed with less than 30 samples were excluded.

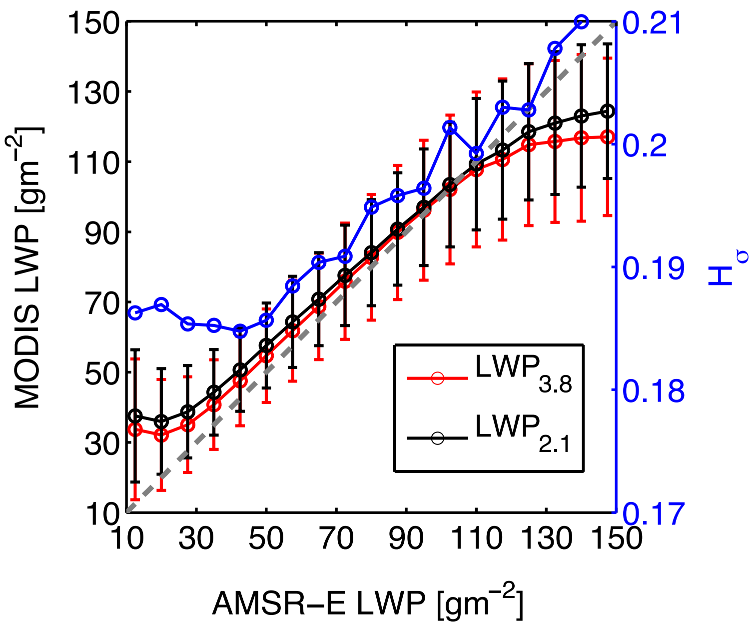

Fig. 4. MODIS LWP (red and black lines) and H_σ (blue line) binned as a function of AMSR-E LWP only (left and right axis, respectively). Red and black lines correspond to the binned MODIS LWP$_{3.8}$ and LWP$_{2.1}$, respectively, whereas the error bars denote the standard deviation. The dashed gray line is the 1 : 1 relationship.

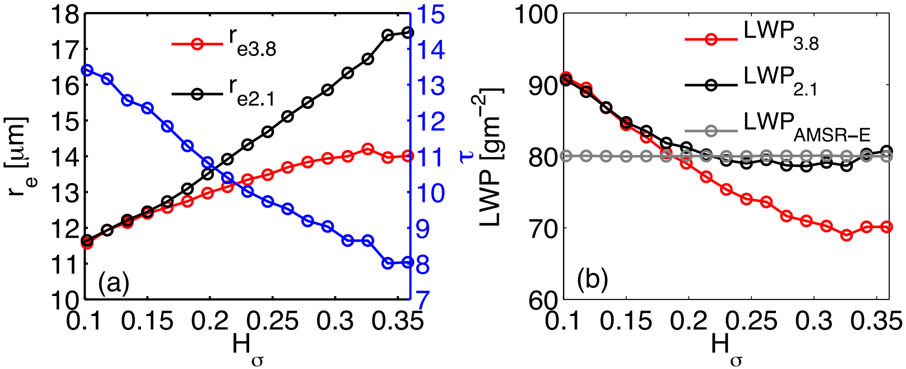

Fig. 5. (a) $r_{e3.8}$, $r_{e2.1}$, and τ binned by AMSR-E LWP and H_σ, and subsequently averaged for all LWP bins (red, black, and blue lines, respectively). **(b)** As in Fig. 5a, but for LWP (AMSR-E LWP is constant at 80 g m^{-2} by design).

ACPD

13, 12725–12742, 2013